Scripta Materialia 155 (2018) 26–31

Contents lists available at ScienceDirect

Scripta Materialia

journal homepage: www.elsevier.com/locate/scriptamat

Regular article

Ultrastrong nanocrystalline stainless steel and its Hall-Petch relationship in the nanoscale

Fei Yin [a,b], Gary J. Cheng [c], Rong Xu [d], Kejie Zhao [d], Qiang Li [e], Jie Jian [e], Shan Hu [a], Shaoheng Sun [a], Licong An [a], Qingyou Han [a,b,*]

[a] School of Engineering Technology, Purdue University, West Lafayette, IN 47907, USA
[b] Brick Nanotechnology Center, Purdue University, West Lafayette, IN 47907, USA
[c] School of Industrial Engineering, Purdue University, West Lafayette, IN 47907, USA
[d] School of Mechanical Engineering, Purdue University, West Lafayette, IN 47907, USA
[e] School of Materials Engineering, Purdue University, West Lafayette, IN 47907, USA

ARTICLE INFO

Article history:
Received 18 April 2018
Received in revised form 4 June 2018
Accepted 6 June 2018
Available online 14 June 2018

Keywords:
Hall-Petch equation
Nanocrystalline stainless steel
Surface mechanical attrition treatment
Nanohardness
Micropillar compression

ABSTRACT

An ultrastrong nanocrystalline stainless steel with a yield strength of ~2.0 GPa was reported and the Hall-Petch equation of the stainless steel in the nanoscale was determined. The effects of the grain refinement and element segregation on the mechanical behaviors of the nanocrystalline stainless steel were analyzed and discussed. The validated Hall-Petch equation for the stainless steel in the nanoscale regime could provide a guideline for Hall-Petch strengthening of the stainless steel with grain refinement.

Nanocrystalline metallic materials exhibit extraordinary mechanical, biological and chemical properties. The mechanical strength of the metallic materials could be adjusted by modulating their grain structure and element segregation at the grain boundaries. According to the classical Hall-Petch equation [1, 2], the yield strength is inverse to the square root of the grain size of the materials. Grain boundary can block the dislocation movement and result in dislocation pile-up when the materials undergo plastic deformation. 316L stainless steel (316L SS) is widely used in the fields of biomedical engineering, structural engineering and civil engineering, et al. due to its good biocompatibility, excellent corrosion resistance and good formability. However, one of the drawbacks of the 316L SS is the low mechanical strength. The yield strength and ultimate strength of the 316L SS is about 250 MPa and 515 MPa, respectively [3]. Grain refinement has been used for the mechanical strengthening of the 316L SS for decades.

For example, Chen et al. developed a nanocrystalline 316L SS (NC-316L SS) with an average grain size of 40 nm. The nanohardness and yield stress of this NC-316L SS is 4.5 GPa and 1.45 GPa, respectively, which are 5 times higher than that of the coarse-grained 316L SS (CG-316L SS) [3]. Roland et al. also developed a NC-316L SS whose strength is comparable to titanium alloys. The developed NC-316L SS could have a yield stress varying from 1.4 GPa to 1.8 GPa [4]. Wang et al. fabricated a NC-316L SS with an average grain size of 62 nm through the high-pressure torsion (HPT) and the yield strength of this NC-316L SS is 1360 MPa. Furthermore, they found the post-deformation annealing could introduce further strengthening to the NC-316L SS. The yield strength of the annealed NC-316L SS can be 2230 MPa [5]. The extra strengthening of the NC-316L SS after annealing could be attributed to the element segregation and nanoscale grain boundary stabilization. Abramova et al. directly observed the Mo-Cr-Si rich grain boundary segregation in the NC-316L SS deformed at elevated temperature (673 K). They demonstrated that the grain boundary segregation can lead to significant enhancement of the yield stress in the NC-316L SS. In their study, the average grain size of the NC-316L SS fabricated at the room temperature and elevated temperate (673 K) is 40 nm and 90 nm, respectively. Both of the NC-316L SS have an enhanced yield strength about 1700 MPa [6]. However, the mechanical behavior of the NC-316L SS with an average grain size smaller than 30 nm has not been reported yet. Investigation of the Hall-Petch relationship of the NC-316L SS in the nanoscale regime is meaningful for the future grain refinement and mechanical strengthening of the austenite 316L SS.

In this study, the NC-316L SS with the average grain sizes varying from 10 nm to hundreds of nanometers was successfully fabricated by surface mechanical attrition treatment (SMAT) at room temperature

* Corresponding author at: School of Engineering Technology, Purdue University, West Lafayette, IN 47907, USA.
E-mail address: hanq@purdue.edu (Q. Han).

https://doi.org/10.1016/j.scriptamat.2018.06.014
1359-6462/

[7–14]. Fifty steel shots with the diameter of 3 mm were accelerated by a vibrating solid surface driven by high frequency ultrasonic signal in an enclosed chamber. The multidirectional impacts of the shots on the 316 L stainless steel surface resulted in the grain refinement of the materials. The working distance and peening time is 10 mm and 600 s, respectively. A NC-316L SS (~25 nm) structure with a yield strength of 1.91 GPa, which is the highest ever reported in the literatures for the NC-316L SS deformed at room temperature and without post-heat treatment, was identified by micro-pillar compression test and validated by the nanohardness tests. Even higher yield stress, namely 2.0 GPa, is guaranteed on the NC-316 L SS with the average grain size of 15 nm at the topmost surface according to the nanohardness measurements.

Fig. 1(a) is the Scanning Electron Microscope (SEM) characterizations of the etched NC-316L SS from the cross-sectional direction. The NC-316L SS specimen was polished by using diamond pastes firstly, and then etched at room temperature in a solution of 20 ml nitric acid, 20 ml hydrochloric acid and 20 ml distilled water. Fig. 1 (b) illustrates the gradient NC-316L SS surface layer characterized by means of the Focus Ion Beam (FIB) channeling contrast image technique [15–17]. The average grain size of the NC-316L SS increases gradually with the increment of the depth from the topmost surface. The extremely fine NC-316L SS structure was characterized by Transmission Electron Microscope (TEM) as shown in the Fig. 1(c). The average grain size of this surface layer (~3 μm thick) is around 10 nm according to the statistical analysis of the characterization results. The TEM sample was prepared by the FIB and lift-Out method by using the FEI QUANTA 3D FEG SEM/FIB equipped with the Omniprobe AutoProbe 200 lift-out system and characterized by using an FEI Tecnai TEM operated at 200 kV. With the increment of the depth from the topmost surface to 15 μm, the average grain size of the gradient NC-316L SS surface layer increases from 10 nm to 115 nm gradually as illustrated in the Fig. 1 (c)–(e). It should be noted that there is no observation of twin boundaries in the nano-structures closing to the topmost surface as illustrated in the Fig. 1(c)–(d). Nevertheless, there are many twins in the large grains deep in the matrix as shown in the Fig. 1(a). The twin structure may be further refined into extremely fined nanocrystalline structure because of the continuous high strain-rate impacts.

Fig. 2(a) shows the nanohardness of the gradient NC-316L SS at the location of 2 μm, 4 μm, 8 μm, 12 μm, 16 μm and 20 μm depth from the topmost surface with their corresponding average grain sizes of 15 nm, 25 nm, 42 nm, 58 nm, 115 nm and 168 nm, respectively. The average grain size of the materials at different location was measured based on the FIB channeling contrast imaging and TEM characterization as illustrated in the Fig. 1. The nanohardness of the NC-316L SS was measured by using the Agilent Technologies Nanoindenter G200 with a standard Berkovich diamond indenter. Mechanical properties including nanohardness and elastic modulus were obtained from force-displacement curves by standard Oliver and Pharr method [18]. The maximum displacement of the indentations is 500 nm. The loading, holding, and unloading times were 20 s, 5 s, and 20 s, respectively. The maximum nanohardness of the NC-316L SS is 6.093 GPa located at the layer of around 2–3 μm depth from the topmost surface with the average grain size of 15–20 nm. The nanohardness of the NC-316L SS with the average grain sizes of 25 nm, 42 nm, 58 nm, 115 nm and 168 nm is 5.875 GPa, 5.77 GPa, 5.57 GPa, 5.44 GPa and 5.356 GPa, respectively. Eq. (1) reflects the relationship between the grain size and hardness of the materials with regard to the well-established Hall-Petch Eq. (4):

$$H_v = H_0 + \frac{K_h}{\sqrt{d}} \tag{1}$$

where, H_v is the hardness of a materials; H_0 and K_h are the materials constants; d is the average grain size of the materials. Also, the empirical relationship between the hardness and yield stress of the material can be seen in the Eq. (2):

$$H_v = 3\sigma_y \tag{2}$$

where the σ_y is the yield stress of the materials and could be expressed as follows:

$$\sigma_y = \sigma_0 + \frac{K_y}{\sqrt{d}} \tag{3}$$

where σ_0 is the friction stress and K_y is a yield constant.

Furthermore, to get the yield strength and flow behavior of the NC-316L SS, micropillar compression tests were performed. Micropillars with the diameter of ~3 μm and length of ~6 μm were fabricated by using the FIB in the FEI Nova 200 SEM/FIB Dual beam system. The

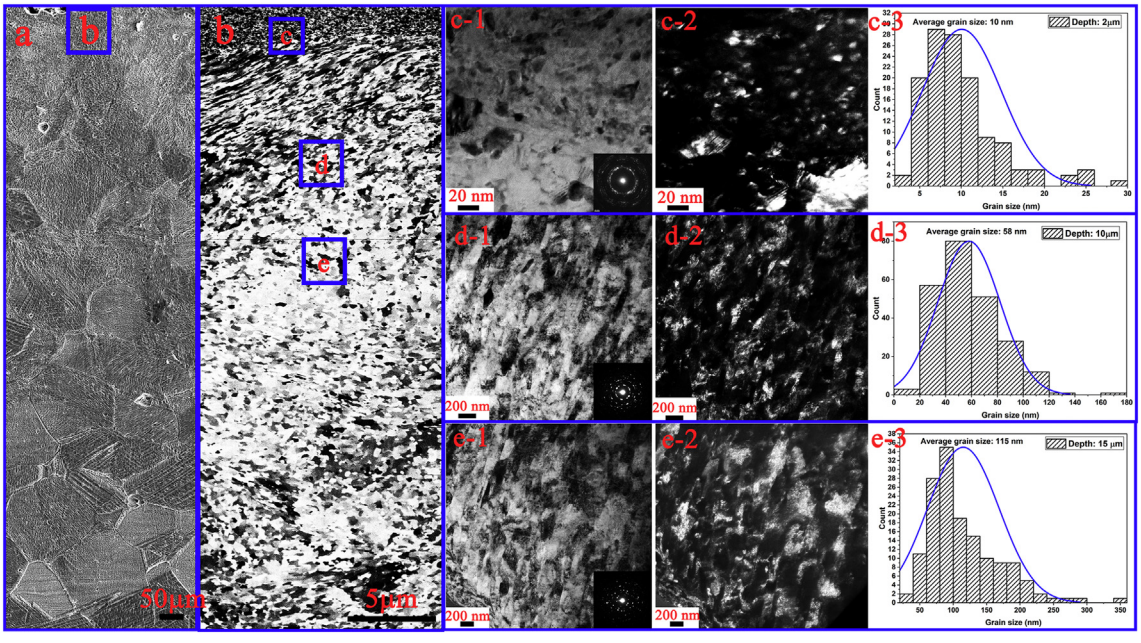

Fig. 1. Characterizations of the gradient nanocrystalline 316L stainless steel and the grain size distribution along the cross-sectional direction in the nanoscale.

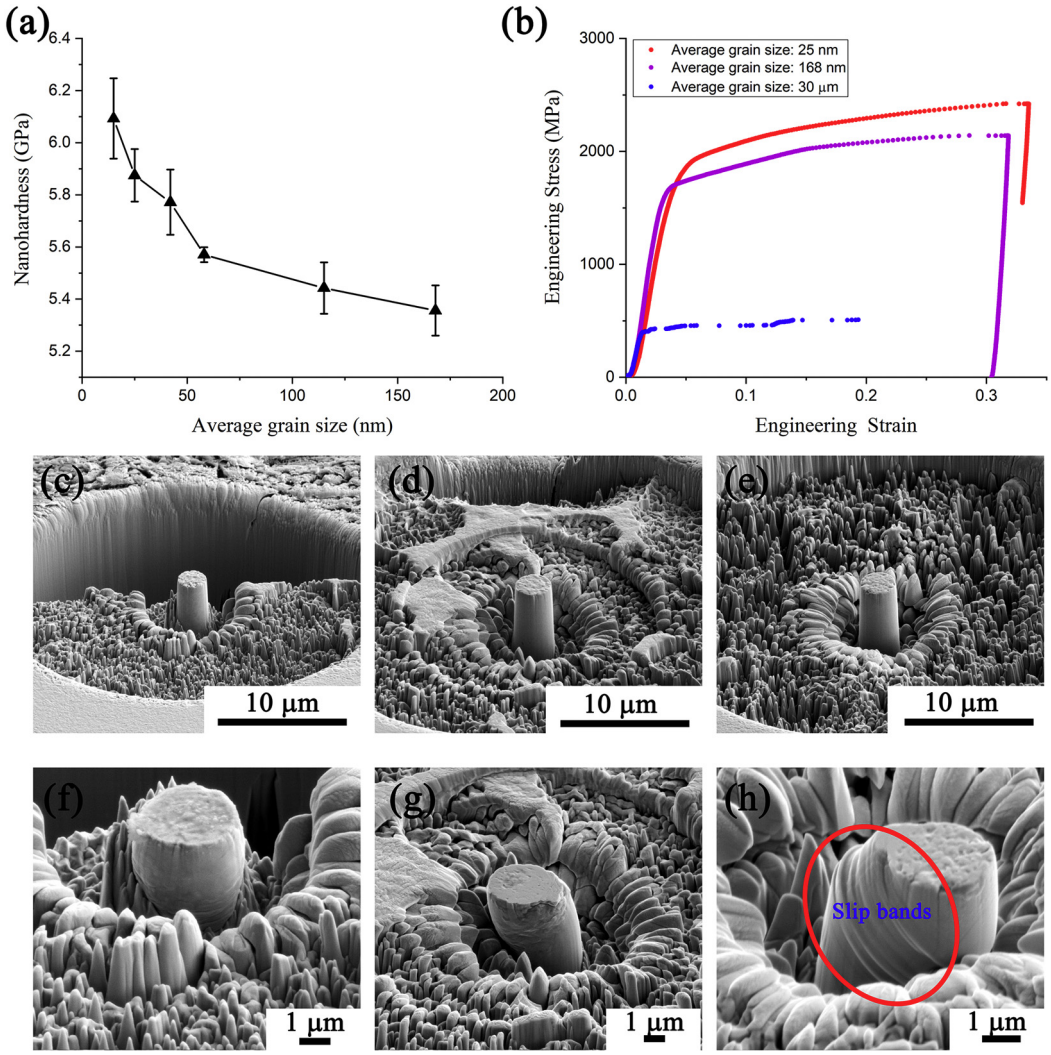

Fig. 2. (a) Nanohardness of the nanocrystalline 316L stainless steel (NC-316L SS) with different grain size in the nanoscale and (b) the stress-strain curves of the NC316L SS micropillar with the average grain size of 25 nm, 168 nm and 30 μm; The micro-pillars fabricated on the NC-316L SS (c, d, e) before and (f, g, h) after micro-pillar compression tests with the average grain size of 25 nm, 168 nm and 30 μm, respectively. (The micro-pillars were captured with a stage tilt of 52° by using SEM).

positions of the micropillars were precisely controlled at the locations of 5 μm, 20 μm and 1500 μm depth from the topmost surface. Then, the micro-pillar compression tests were conducted on the AGILENT Technologies Nanoindenter G200 with a diamond flat tip. The entire displacement of the tip is 2000 nm with the average strain rate of 0.01 s^{-1}. Fig. 2(b) shows the engineering stress-strain curves of the micropillar compression tests at the surface layer with the average grain size of 25 nm, 168 nm and 30 μm. The yield stress of the NG-316L stainless steel with the average grain size of 25 nm and 168 nm is 1.906 GPa and 1.716 GPa, respectively. The corresponding nanohardness is 5.875GPa and 5.356 GPa, respectively. The nanohardness and yield strength agree pretty well with the empirical equation as shown in the Eq. (2) with an error of 2.66% and 3.87%, which implies that the fabricated NC-316L SS is fully dense and free of porosity.

The engineering stress-strain curves for the nanograined micropillars are smooth and the flow stress includes an elastic region and work hardening region. There are some visible strain avalanches in the stress-strain curve of the coarse-grained micropillar. The strain avalanche is a well-known phenomenon characterizing the plasticity of micropillars of single crystals and/or coarse-grained crystals, where complex dislocation processes take place intermittently causing scale-free isolated slip events [19]. The microstructure of the nanograined and coarse-grained micro-pillars before and after compression tests were illustrated in the Fig. 2(c)–(h). It can be seen in the Fig. 2(f) and (g) that there are no slip bands on the surface of the deformed micro-pillar. However, slip bands were characterized at the surface of the deformed pillar in the Fig. 2(h) and dislocation movements dominate during the plastic deformation of the coarse-grained micro-pillar [20]. Note that the micropillars in this study have an average diameter of ~3 μm, which led to negligible "size effect" that has taken place in single- and coarse-grained crystals. The abundant boundaries that originated from dislocation cell structures during SMAT process as well as high density dislocation tangles within grain interiors greatly strengthen the NC-316L SS. The strain hardening in compression experiments at higher stain level is ascribed to dislocation interactions and the occurrence of dislocation cross-slip might leave extra room for hardening.

Based on the nanohardness and yield strength of the NC-316L SS, the Hall-Petch equation of the NC-316L SS in nanoscale was fitted and compared with the previously published data in the Fig. 3. Table 1 lists the published nanohardness or yield strength data of the NC-316L SS with different grain sizes, heat-treatment conditions and phase conditions.

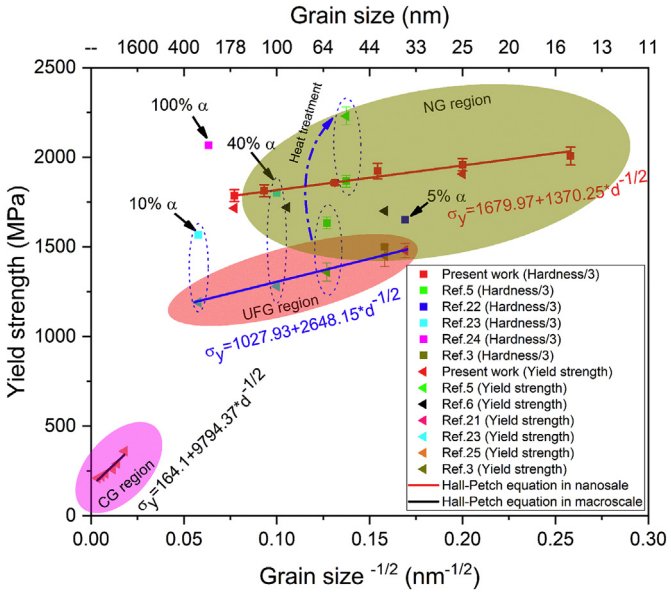

Fig. 3. Plot of the yield strength and nanohardness (H/3) as a function of the inverse square root of mean grain size of the 316L stainless steel using results reported in the literatures and in this study (CG: coarse-grained; UFG: ultrafine grained; NG: nanograined).

It can be seen in Fig. 3 that the Hall-Petch equation of the NC-316L SS in the nanoscale developed in this study agrees pretty well with the theoretical linear equation. And the Hall-Petch equation of the NC-316L SS in the nano-scale was determined as shown in the Eq. (4):

$$\sigma_y = 1679.97 + 1370.25 * d^{-1/2} \quad (4)$$

where σ_y is the yield strength of the NC-316L SS and d is the average grain size of the NC-316L SS.

Furthermore, the Hall-Petch equations of the NC-316L SS in the coarse-grained (CG) scale and ultra-fine grained (UFG) scale were fitted by using the previously published data as illustrated in the Fig. 3 as well. And the yield constant k_y of the NC-316L SS in the CG scale, UFG scale and NG scale is 9794.37 MPa $nm^{-1/2}$, 2648.15 MPa $nm^{-1/2}$ and 1370.25 MPa $nm^{-1/2}$, respectively. The decrease of the yield constant of the nanocrystalline metallic materials is resulted from the grain size dependence of the stress required to operate a Frank-Read source [26] and the strong reduction in the numbers of dislocations in the pile-ups with decreasing grain size [27]. The similar difference between the Hall-Petch parameters for coarse-grained and ultrafine grained regimes in the 316L SS was identified by Gubicza et al. [28].

In addition, the phase condition could affect the mechanical strength of the UFG/NG-316L SS as illustrated in the Fig. 3. The 100% α phase with the average grain size of 250 nm has a highest hardness of 6.2 GPa as indicated by the arrow in the Fig. 3. Nevertheless, Gubicza pointed out that the grain size has a more deterministic effect on the strength of the UFG/NC-316L SS compared with the influence of the phase composition [28]. In the present study, the XRD profile indicates a mixture α and γ phase in the NC-316L SS. The yield strength measured by Ucok et al. in the NC-316L SS was circled by the blue dash lines in the Fig. 3. It should be noted that the error between the nanohardness/3 and the yield strength of the data is significant. That could be explained by the porosity of the 316L stainless steel fabricated by the liquid dynamic compaction method [23].

The yield strength of the NC-316L SS could also be affected by the element segregation at nanoscale grain boundaries. Hu et al. indicated that the strength of the materials could be modulated by tailoring the element segregation at the nano-scaled grain boundaries. They strengthened the nanocrystalline Ni alloy by tailoring the content of the Mo and promoting the Mo segregation at the nano-scaled grain boundaries [29].

Table 1
Data of the yield strength and/or nanohardness of the coarse-grained, ultrafine grained and nanograined 316L stainless steel in the literatures and in this study.

Processing method	Phase condition	Average grain size	UTS (MPa)	Yield strength (MPa)	Elongation (%)	Hardness (HV10/GPa)	References
SMAT	α + γ	15 nm	–	–	–	6.0193 ± 0.15	Present work
SMAT	α + γ	29 nm	–	1906	–	5.875 ± 0.1	Present work
SMAT	α + γ	42 nm	–		–	5.77 ± 0.13	Present work
SMAT	α + γ	58 nm	–			5.57 ± 0.03	Present work
SMAT	α + γ	115 nm	–		–	5.44 ± 0.1	Present work
SMAT	α + γ	168 nm		1716	–	5.356 ± 0.1	Present work
HPT at RT	100% γ	62 nm	1790 ± 50	1360 ± 50	22.9 ± 0.2	4.9 ± 0.1	[5]
HPT at RT + 773 K/1 h	100% γ	53 nm	2390 ± 50	2230 ± 50	16.1 ± 0.2	5.6 ± 0.1	[5]
HTP at RT	α + γ	40 nm	–	1700	–	–	[6]
HTP at 673 K	α + γ	90 nm	–	1720	–	–	[6]
ECAP at 423 K with 4 passes	–	30–40 nm (inter-twin spacing)	1560 ± 40	1480 ± 40	0.5–1.6	–	[21]
95% CR at 258 K + 1023 K/300 s	95% γ	150 ± 50 nm	1270	–	–	–	[22]
95% CR at 273 K + 1023 K/300 s	95% γ	300 ± 50 nm	1251	–	–	–	[22]
7% CR at 523 K +95% CR at 258 K + 1023 K/300 s	95% γ	100 nm	1304	–	–	–	[22]
30% CR at 523 K + 95%CR at 258 K +1023 K/300 s	95% γ	35 ± 5 nm	1385	–	5.5	495 HV	[22]
80% CR at 77 K	100% α	–	1920	1670	2.9	5.6 Gpa	[23]
80% CR at 77 K + 873 k/600 s	40% α	100 nm	1610	1280	3.2	5.4 Gpa	[23]
80% CR at 77 K + 973 k/600 s	10% α	300 nm	1400	1190	5	4.7 GPa	[23]
90% CR at 298 K	γ	–	1380	1290	3.2	4.5 GPa	[23]
50% HR at 1437 K + 80% CR at 298 K	γ	–	1450	1290	6	–	[23]
MM + 1173 K/3.6 ks VHP	100% α	250 nm	–	–	–	6.2 GPa	[24]
90% CR at 298 K + annealed	γ	3.1 μm	–	360	–	–	[25]
90% CR at 298 K + annealed	γ	5.1 μm	–	290	–	–	[25]
90% CR at 298 K + annealed	γ	7.3 μm	–	260	–	–	[25]
90% CR at 298 K + annealed	γ	16.8 μm	–	235	–	–	[25]
90% CR at 298 K + annealed	γ	33 μm	–	220	–	–	[25]
90% CR at 298 K + annealed	γ	87 μm	–	210	–	–	[25]
Coarse grained	γ	20 μm	630	250	55	2 GPa	[3]
SMAT	γ	40 nm	1550 ± 80	1450 ± 60	3.4	4.5 GPa	[3]

RT: room temperature; CR: cold rolling; HPT: high pressure torsion; MM: mechanical milling; VHP: vacuum hot pressing; UTS: ultimate tensile strength; SMAT: surface mechanical attrition treatment.

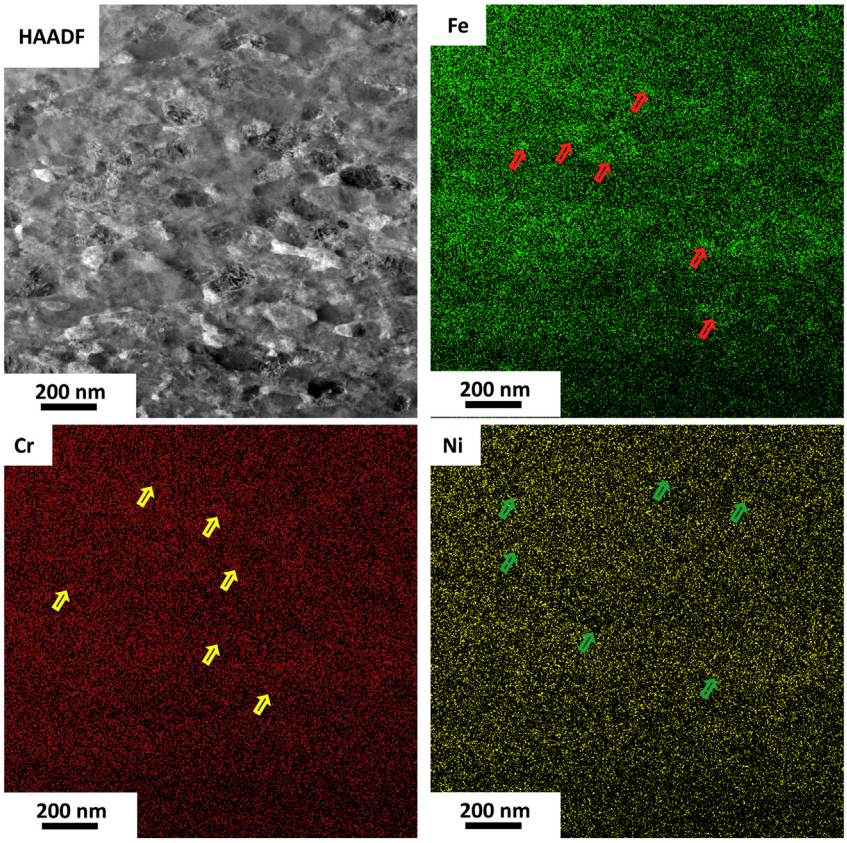

Fig. 4. (a) HAADF-STEM image and EDS elemental maps showing the spatial distribution of (b) Fe, (c) Cr and (d) Ni of the NC-316L SS.

The further mechanical strengthening of the NC-316L SS has been achieved by Wang et al. by using a post-deformation-annealing treatment of the NC-316L SS fabricated by HPT method as illustrated in the Fig. 3. They stated that the element segregation at the grain boundaries could be the reason for the further mechanical strengthening of the NC-316L SS [5]. However, Renk et al. pointed out that the further strengthening of the NC-316L SS after annealing is not related to solute segregation and not to second-phase particles at the boundaries. The further hardening effect during annealing of the NC-316L SS can be attributed to the annihilation of relatively mobile dislocation and a relaxation of the grain boundaries, making emission of dislocations or their relaxation at the boundary difficult [30]. To identify the effect of the element segregation on the mechanical strengthening of the NC-316L SS in this study, the element distribution of the NC-316L SS was analyzed by using a FEI Talos 200X TEM microscope (FEI, USA) equipped with an FEI Super-X™ detector system, which combines four symmetrically positioned Si drift detectors (SDD) around the objective lens with a high-brightness gun as detailed in a recent publication [31, 32]. Fig. 4(a) shows the High Angle Annular Dark Field (HAADF) STEM imaging of the NC-316L SS. Fig. 4(b)–(d) illustrate the EDS mapping of the NC-316L SS for the elements Fe, Cr and Ni. It can be seen in the Fig. 4 that element (Fe, Cr, Ni) segregation as indicated by the colored arrows were successfully identified in the nanocrystalline materials, which could result in solute pinning effect on retarding dislocation movement and grain boundary stability. We believe that the nanosized grains and the element segregation in the nanoscale both contribute to the ultra-high yield strength of the nanocrystalline 316L stainless fabricated in this study.

In closing, this study reported an ultrastrong NC316L SS with the yield strength of 2.0 GPa and determined the Hall-Petch equation of the NC-316L SS in the nanoscale. The mechanical strengthening mechanisms for the NC-316L SS fabricated in this study were discussed and analyzed and the element distribution of the developed NC-316L SS was carefully examined and measured. For future investigation, high resolution TEM can be conducted to analysis the dislocation boundary characteristics for an in-depth understanding of the strengthening mechanism of the gradient nanocrystalline 316L stainless steel developed in this study [33, 34]. In general, the developed Hall-Petch equation for the NC-316L SS in nanoscale will provide a solid guideline for the study of the mechanical strengthening of the NC-316L SS in the future investigations.

References

[1] N.J. Petch, J. Iron Steel Inst. Jpn. 174 (1953) 25.
[2] E. Hall, Proc. Phys. Soc. London, Sect. B 64 (1951) 747.
[3] X. Chen, J. Lu, L. Lu, K. Lu, Scr. Mater. 52 (2005) 1039.
[4] T. Roland, D. Retraint, K. Lu, J. Lu, Mater. Sci. Eng. A 445 (2007) 281.
[5] H. Wang, I. Shuro, M. Umemoto, K. Ho-Hung, Y. Todaka, Mater. Sci. Eng. A 556 (2012) 906.
[6] M. Abramova, N. Enikeev, R. Valiev, A. Etienne, B. Radiguet, Y. Ivanisenko, X. Sauvage, Mater. Lett. 136 (2014) 349.
[7] F. Yin, S. Yang, S. Hu, S. Kuang, Q. Han, Mater. Lett. 189 (2016) 275.
[8] F. Yin, M. Rakita, S. Hu, H.M. Sertse, Q. Han, J. Manuf. Process. 26 (2017) 393.
[9] F. Yin, Q. Han, M. Rakita, M. Wang, L. Hua, C. Wang, Int. J. Comput. Mater. Sci. Surf. Eng. 6 (2015) 97.
[10] F. Yin, L. Hua, X. Wang, M. Rakita, Q. Han, Comput. Mater. Sci. 92 (2014) 28.
[11] F. Yin, M. Rakita, S. Hu, Q. Han, Surf. Eng. 1 (2017).
[12] F. Yin, S. Hu, L. Hua, X. Wang, S. Suslov, Q. Han, Metall. Mater. Trans. A 46 (2015) 1253.
[13] Q. Han, Metall. Mater. Trans. B Process Metall. Mater. Process. Sci. 46 (2015) 1603.
[14] M. Rakita, M. Wang, Q. Han, Y. Liu, F. Yin, Int. J. Comput. Mater. Sci. Surf. Eng. 5 (2013) 189.
[15] M. Uchic, M. Groeber, D. Dimiduk, J. Simmons, Scr. Mater. 55 (2006) 23.
[16] S. Canovic, T. Jonsson, M. Halvarsson, J. Phys. Conf. Ser. 126 (2008) 1–4 012054.
[17] M. Phaneuf, Micron 30 (1999) 277.
[18] W.C. Oliver, G.M. Pharr, J. Mater. Res. 7 (1992) 1564.
[19] N.Q. Chinh, T. Györi, R.Z. Valiev, P. Szommer, G. Varga, K. Havancsák, T.G. Langdon, MRS Commun. 2 (2012) 75.
[20] J.R. Greer, J.T.M. De Hosson, Prog. Mater. Sci. 56 (2011) 654.
[21] H. Ueno, K. Kakihata, Y. Kaneko, S. Hashimoto, A. Vinogradov, Acta Mater. 59 (2011) 7060.
[22] M. Eskandari, A. Najafizadeh, A. Kermanpur, Mater. Sci. Eng. A 519 (2009) 46.

[23] İ. Üçok, T. Ando, N.J. Grant, Mater. Sci. Eng., A, 133 (1991) 284.
[24] H. Fujiwara, K. Ameyama, Mater. Sci. Forum (1999) 47.
[25] B. Kashyap, K. Tangri, Acta Mater. 43 (1995) 3971.
[26] Y. Estrin, H. Kim, F. Nabarro, Acta Mater. 55 (2007) 6401.
[27] N.Q. Chinh, J. Gubicza, T. Langdon, J. Mater. Sci. 42 (2007) 1594.
[28] J. Gubicza, M. El-Tahawy, Y. Huang, H. Choi, H. Choe, J.L. Lábár, T.G. Langdon, Mater. Sci. Eng. A 657 (2016) 215.
[29] J. Hu, Y. Shi, X. Sauvage, G. Sha, K. Lu, Science 355 (2017) 1292.
[30] O. Renk, A. Hohenwarter, K. Eder, K. Kormout, J. Cairney, R. Pippan, Scr. Mater. 95 (2015) 27.
[31] A. Genc, L. Kovarik, M. Gu, H. Cheng, P. Plachinda, L. Pullan, B. Freitag, C. Wang, Ultramicroscopy 131 (2013) 24.
[32] C.-M. Wang, A. Genc, H. Cheng, L. Pullan, D.R. Baer, S.M. Bruemmer, Sci. Rep. 4 (2014) 3683.
[33] N. Hansen, Scr. Mater. 51 (2004) 801.
[34] X. Zhang, N. Hansen, Y. Gao, X. Huang, Acta Mater. 60 (2012) 5933.